MIJST
MIST International Journal of Science and Tenchnology

RANS Flow Computation around Transonic RAE2822 Airfoil with a New SST Turbulence Model

Md Mizanur Rahman[1*], Xueting Zhang[2], K. Hasan[3], and Sheng Chen[4]

School of Mechanical Engineering, Hangzhou Dianzi University, Zhejiang, China

email: *[1]mizanur_rahman@hdu.edu.cn, [2]zxt@hdu.edu.cn, [3]m.k.hasan@hdu.edu.cn, and [4]chensh@hdu.edu.cn*

ARTICLE INFO

Article History:

Received: 30rd July 2024
Revised: 12th November 2024
Accepted: 17th November 2024
Published: 26th December 2024

Keywords:

Occupational Risk
Risk Management
Shipbuilding Industry
Hazards in Shipbuilding
Workplace Safety Regulations

ABSTRACT

The solution to RANS (Reynolds-averaged Navier-Stokes) equations invokes a suitable framework for turbulence modelling. To account for turbulence and transition effects, a new SST (Shear Stress Transport) $\boldsymbol{k-\omega}$ turbulence model is coupled with RANS to simulate the transonic flow passing an RAE2822 air foil. Three sets of experimental data of the super-critical RAE2822 air foil are employed to validate the new SST (NSST) closure. Computations are conducted for a limited range of Reynolds numbers with variable angle of attack. The NSST model has been found to replicate satisfactory results for lift $\boldsymbol{C_L}$ and drag $\boldsymbol{C_D}$ coefficients as well as for skin-friction and pressure coefficient profiles under considerable shock-wave boundary layer (BL) interaction, although $\boldsymbol{C_D}$ is challenging to be accurately predicted since the turbulence model requires to adequately resolve near-wall turbulence in the BL with varying pressure gradients. NSST predictions are compared with those of the widely-used SST $\boldsymbol{k-\omega}$ model. Numerical outputs demonstrate that the included NSST transition model plays no significant roles to appropriately predict $\boldsymbol{C_L}$ and $\boldsymbol{C_D}$, indicating that the NSST performance is almost equivalent to that of the SST in the current analysis.

NOMENCLATURE

c	airfoil cord length
C_f	skin-friction coefficient
C_D	drag coefficient
C_L	lift coefficient
C_μ	closure coefficients
k	turbulent kinetic energy
R_T	eddy-to-laminar viscosity ratio
Ma	Mach number
$NSST$	new SST
R_b	stress intensity parameter
P_k	turbulent production
y^+	dimensionless wall distance
γ	turbulence intermittency
θ	momentum thickness
μ	dynamic viscosity
μ_T	turbulent eddy-viscosity
ν	kinematic viscosity $\left(\frac{\mu}{\rho}\right)$
ν_T	kinematic eddy-viscosity $\left(\frac{\mu_T}{\rho}\right)$
ρ	density
$\sigma_{k,\omega}$	Schmidt numbers
ω	specific dissipation rate

Subscript:

i, j	variable quantities
∞	free-stream/reference condition

1. INTRODUCTION

The transonic flow over air foils has gained considerable attention due to the shock-wave interactions with the turbulent boundary layer (BL) which invoke flow separation, shock unsteadiness and modification to the shock structure. For a constant free-stream Mach number (Ma) with variable Angle of Attack (AOA), three types of transonic shock-wave BL interactions may exist [1] in typical industrial applications. A weak shock-wave forms with a low AOA which results in a thickened attached BL and pressure fluctuation levels are insignificant upstream of the interaction. However, an intermediate AOA may strengthen the shock wave, giving rise to a separation zone at the foot of shock. The flow regions adhering to upstream of the shock and downstream of the separation bubble may experience insignificant levels of unsteadiness. The strong shock appears with a high AOA, forming a separation bubble which extends from the shock foot to the trailing edge. It is worth mentioning that these types of shock-wave BL interactions can be confronted for a constant AOA with variable free-stream Ma.

The transonic flow over RAE2822 air foil can be a standard validation case to justify numerical computations since comprehensive measured data achievable for this air foil [2-7]. Information from the upstream condition is used to compute mean flow parameters, although the velocity exceeds the speed of sound in regions of transonic flows. In addition, the source terms of turbulence models may confront strong spatial gradients due to the appearance of shock waves in the flow [3]. These features raise the questions of whether the turbulence models are capable of representing transonic flows and how accurately the shock location in flows involving "shockwave BL interactions" with flow separation near the shock foot are predicted. Endeavours to compute flow past an RAE2822 air foil using various turbulence models with the wind tunnel correction and far-field vortex effects, even by altering Ma and AOA have been less than satisfactory [5].

The overall disagreement pattern shows the well-predicted shock at the measured location, the over-predicted "post-shock pressure recovery" on the upper (suction) surface, and the under-predicted "roof-top pressure" recovery by some turbulence models and over-predicted by other closures [5-9]. Apparently, the test case is challenging in the context of producing accurate simulations and worthy of attention to typical industrial applications. The appearance of transonic "shock-wave BL interactions" at an air foil surface results in a degraded performance. However, the lost efficacy could be retrieved to an extent with a super-critical air foil like an RAE2822, ascertaining a "roof-top type pressure" allotment.

The current effort is to simulate the turbulence and transition (although transition has been tripped in the experiments) around the transonic RAE2822 air foil using a recently devised Shear Stress Transport (SST) $k-\omega$ model in conjunction with RANS (Reynolds-averaged Navier-Stokes equations). In addition, the impact of transition model on the computation of drag and lift coefficients has been evaluated. The new SST (NSST) model [10] mimics the characteristics of both the standard SST $k-\omega$ model [11] and correlation based $\gamma - Re_\theta$ transition model [12].

The NSST model differs from the SST and $\gamma - Re_\theta$ models in several ways: (a) blending functions are avoided; (b) diffusion coefficients meet the requirements, dictating the "asymptotic flow behaviour" at the turbulent/non-turbulent interface; (c) "stress strain misalignment" problem is absent; (d) turbulent production term is independent of the Reynolds-stress $\overline{u_i u_j}$ tensor and (e) NSST is an algebraic transition model. Remarkably, classical BL flows are used to calibrate the $\gamma - Re_\theta$ transition model and corrections to the underlying correlations may be required when applying the transition model to this transonic wall-bounded test case. Therefore, computations from the standard SST model are compared with those of the NSST model and the impact of adding the transition model on the present set of computations has been quantified.

2. TURBULENCE AND TRANSITION MODELING

The NSST $k-\omega$ closure is employed to handle turbulence and transition; the NSST model can be represented as follows:

$$\frac{D(\rho k)}{Dt} = \frac{\partial}{\partial x_j}\left[(\mu + \sigma_k \mu_T)\frac{\partial k}{\partial x_j}\right] + \rho P_k - \rho C_\mu k\omega \quad (1)$$

$$\frac{D(\rho \omega)}{Dt} = \frac{\partial}{\partial x_j}\left[(\mu + \sigma_\omega \mu_T)\frac{\partial \omega}{\partial x_j}\right] + \rho C_{\omega 1}\frac{P_k}{\nu_T} - \rho C_{\omega 2}\omega^2 + C_\omega \frac{\mu_T}{k}\max\left(\frac{\partial k}{\partial x_i}\frac{\partial \omega}{\partial x_i}; 0\right) \quad (2)$$

Here the material derivative $\frac{D}{Dt} = \frac{\partial}{\partial t + \frac{u_j \partial}{\partial x_j, \rho}}$ the density, u_j the velocity vector, x_j the Cartesian coordinates, k the turbulent kinetic energy, ω the specific dissipation rate, and the kinematic eddy-viscosity $\nu_T = \frac{\mu_T}{\rho}$ with μ_T being the absolute turbulent eddy-viscosity. Model constant coefficients are: $C_\mu = 0.09, \sigma_k = \sigma_\omega = 0.75, C_\omega = 0.25, C_{\omega 1} = 0.5$ and $C_{\omega 2} = 0.075$.

The following relation is used to evaluate the kinematic eddy-viscosity ν_T:

$$\nu_T = \frac{\mu_T}{\rho} = \frac{\tilde{R}_b k}{max(\tilde{R}_b \omega; S)} \quad (3)$$

where $S = \sqrt{2S_{ij}S_{ij}}$ the absolute magnitude of mean strain-rate tensor S_{ij}, calculated as

$$S_{ij} = \frac{1}{2}\left(\frac{\partial u_i}{\partial x_j} + \frac{\partial u_j}{\partial x_i}\right) - \frac{2}{3}\frac{\partial u_k}{\partial x_k}\delta_{ij} \quad (4)$$

where δ_{ij} the Kronecker's delta function. The auxiliary stress intensity factors R_{by} (as a function of turbulent Reynolds number $Re_y = \sqrt{k}y/\nu$, where y the shortest distance to the wall and $\nu = \mu/\rho$ the kinematic laminar viscosity) and $R_\mu = \frac{\nu_T}{\nu}$ (eddy-to-laminar viscosity ratio) constitute the modified stress intensity parameter $\tilde{R}_b$, which can be evaluated as,

$$\tilde{R}_b = min\left(\frac{R_b}{\sqrt{C_\mu}}; a_1\right) \quad (5)$$

where $a_1 = 0.315$ and $R_b = max\left(R_{by}; R_{b\mu}\right)$ with

$$R_{by} = \frac{C_1 Re_y^{0.6}}{\left(1.0 + C_2^2 Re_y^2\right)^{0.3}} \quad (6)$$

$$R_{b\mu} = \frac{C_3 R_\mu^{0.4}}{\left(1.0 + R_\mu\right)^{0.16}\left(1.0 + C_1^2 R_\mu^2\right)^{0.12}} \quad (7)$$

where $C_1 = \frac{C_\mu}{5.0, C_2 = \frac{C_1}{2.0}}$ and $C_3 = C_\mu^{0.9}$. Conventionally, a pre-transition/pseudo-laminar allotment before transition is ensured with $R_\mu < 1.0$, and $R_\mu = 1.0$ regards transition between laminar and turbulence states. Transition triggering is activated by reforming $\tilde{R}_b$ in Eq. (5) as follows:

$$\tilde{R}_b = \begin{cases} min\left(\frac{R_{b\mu}}{\sqrt{C_\mu}}; a_1\right) & \text{if } R_\mu \le 1.0 \\ Eq.(5) & \text{otherwise} \end{cases} \quad (8)$$

Table 1
RAE2822 airfoil: C_L and C_D for Ma = 0.75 at $Re_\infty = 6.2 \times 10^6$

AOA	Parameters	EXPT	SST	NSST
2.72 deg	C_L	0.743	0.722	0.727
–	Err (%)	–	−2.83	−2.15
–	C_D	0.0242	0.0231	0.0230
–	Err (%)	–	−4.55	−4.95

The production term P_k in Eqs. (1) and (2) is evaluated from:

$$P_k = \tilde{R}_b k S \tag{9}$$

It is necessary to stress that the linear Reynolds-stress $\overline{u_i u_j}$ tensor disappears in P_k due to the involvement of the structure parameter $\tilde{R}_b$ and thus, avoiding the "stress-strain misalignment" inconsistency encountered with the "Boussinesq approximation" in relation to the ν_T constitutive formulation. To be concise, compared to the standard SST model, the NSST model (a) avoids blending functions; (b) introduces "flow-structure-adaptive" parameters in the eddy-viscosity formulation and (c) makes the production term independent of the $\overline{u_i u_j}$ tensor.

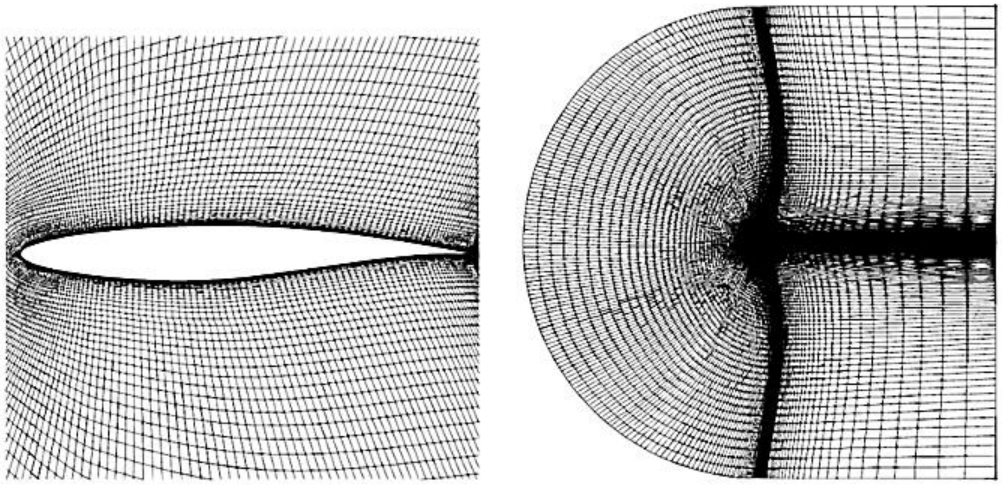

Figure 1: Grid distributions for RAE2822 air foil: (a) near-field view; (b) full view

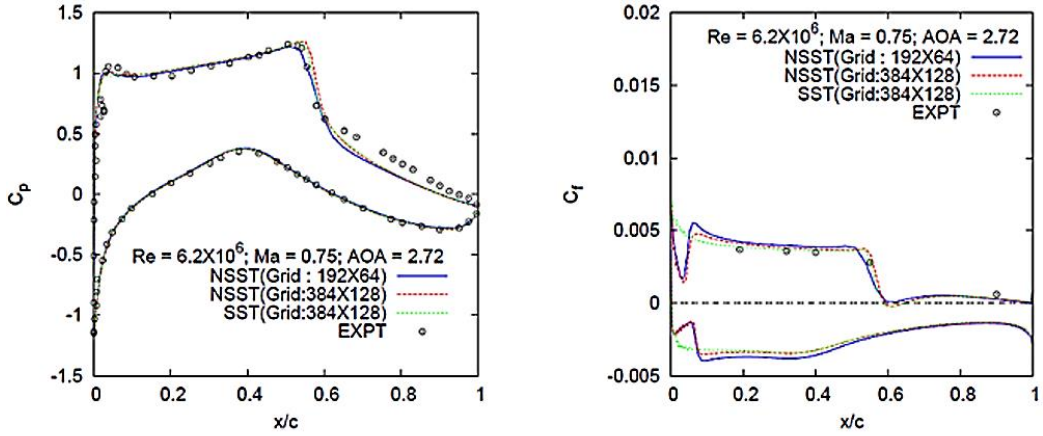

Figure 2: Effect of grid density on RAE2822 air foil simulations with Ma = 0.75 and AOA= 2.72 deg at $Re_\infty = 6.2 \times 10^6$: (a) pressure coefficient profiles; (b) skin-friction profiles

The surface value of ω is based on the surface roughness. Even for a smooth surface a minimum non-dimensional roughness k_{min} is used [13]:

$$k_{min}^{+\left[2.4(y_1^+)^{0.85};8.0\right]} \tag{10}$$

Here $y_1^+ = \frac{y_1 u_\tau}{\nu}$ is the dimensionless distance of the first cell-centre and the wall-friction velocity $u_\tau = \sqrt{\frac{\tau_w}{\rho}}$ with the wall shear stress τ_w. For a rough surface a non-dimensional surface roughness is computed from: $k^+ = (k_R^+; k_{min}^+())$ with the non-dimensional roughness $k_R^+ = \frac{k_R u_\tau}{\nu}$, where k_R is the average sand-grain roughness element height. The wall value of ω is obtained from:

$$\omega_w = \frac{u_\tau^2}{\nu} S_w = S_R S_w \tag{11}$$

where S_w is the strain-rate invariant value at the wall and the factor S_R is used to modify the boundary condition for a rough wall as:

$$S_R = \left[\frac{100}{k^+; \frac{2500}{(k^+)^2}}\right] \tag{12}$$

To enhance proper initialization, the free-stream k (turbulent kinetic energy) and its ω (specific dissipation-rate) are determined as follows [14]:

$$k_\infty = \frac{2}{3}(u_\infty T u_\infty)^2, \quad \omega_\infty = C_\mu \frac{k_\infty}{\nu_{T\infty}} = C_\mu \frac{k_\infty}{\nu_\infty R_{\mu\infty}} \tag{13}$$

where Tu is the turbulence intensity and "∞" indicates free-stream values. Equation (13) is based on the assumption that the k-transport equation deals with the C_μ-based specific dissipation-rate. Therefore, the procedure

provides proper initialization for the computation. The lower limits of ν_T and ω are respectively set as $\nu_T = 10^{-3}\nu_\infty$ and $\omega = \frac{C_\mu u_\infty}{L_\infty}$, where L_∞ is the approximate reference length (could be the length of the computational domain).

3. Numerical simulations

Three representative combinations of available measured data [2-7] are utilized to compute transonic flows over the RAE2822 airfoil with strong shock BL interaction: *(a) Re = 6.2×10^6, Ma = 0.75 & AOA = 2.72 deg; (b) Re = 6.5 × 10^6, Ma = 0.73 & AOA = 2.51 deg and (c) Re = 6.5 × 10^6, Ma = 0.73 & AOA = 2.8 deg*. Transition has been tripped in the experiments along the airfoil surfaces (upper and lower solid boundaries), confined to the Leading Edge (LE) at *x/c = 0.03* (where c the airfoil cord length). The position of the shock and the amount of separation are very dependent on the applied numerical method and turbulence model [3, 5]. A non-uniform *C-type* structured grid *384 × 128* has been created for the RAE2822 airfoil to reproduce better numerical results. Figure 1 displays zoomed and full views of the computational mesh; 256 grid cells lie on the airfoil solid surface, providing the first near-wall cell-height of $y^+ \leq 1.0$. The LE curvature is fairly replicated by carefully arranging mesh points near the LE. The airfoil solid surface deals with viscous wall-boundary conditions. The far-field boundary is located at a distance of 40c in all directions from the airfoil surface, where the external (far-field) boundary conditions are applied with $Tu_\infty = 0.1\%$ (free-stream Tu) and $R_{\mu\infty}$ (free-stream R_μ). Simulations are conducted in a way to match measured coefficients of the lift C_L and drag C_D. Numerical results of the SST $k-\omega$ model is included for comparison purposes. An AC (artificial compressibility) approach in the framework of a cell-centered finite-volume scheme is applied to solve the flow equations. [13-17]. The convective flux is computed using a second-order upwind scheme. Roe's damping term [18, 19] is used to evaluate the flux on the cell face. The iterative solution to the discretized equations employs a time integration method entitled as the diagonally dominant alternating direction implicit (DDADI) scheme. The acceleration of convergence is achieved with a multigrid approach. A detailed implementation of an AC scheme and associated aspects can be found elsewhere [13-17]. An in-house code has been used for the flow simulations and wall-boundary conditions of the NSST model resemble those of the standard SST turbulence closure.

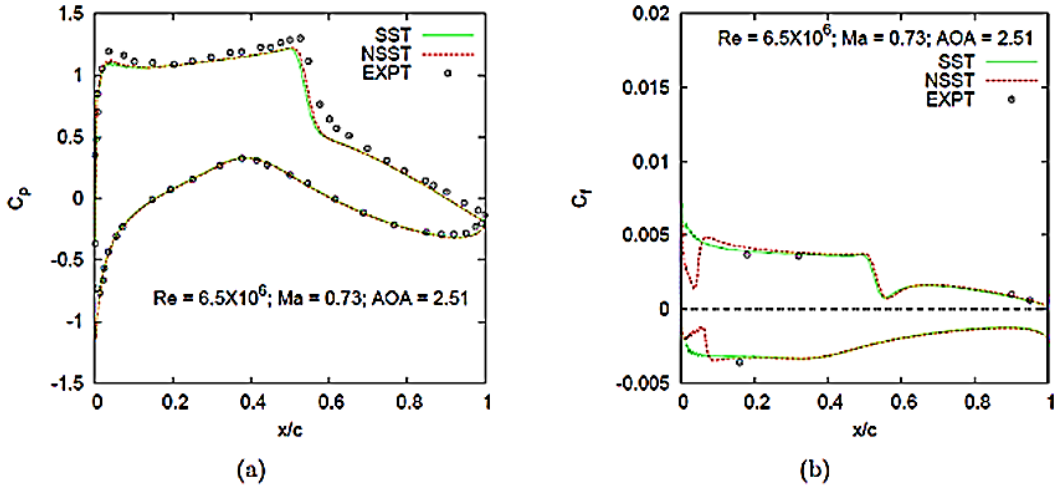

Figure 3: RAE2822 air foil with Ma = 0.73 & AOA= 2.51 deg at $Re_\infty = 6.2 \times 10^6$: (a) C_p profiles; (b) C_f profiles

A grid dependency study has been carried out with the NSST model for the first combination of *Re = 6.2 × 10^6, Ma = 0.75 & AOA = 2.72 deg*. Figure 2 demonstrates C_p and C_f profiles on two grids (allowing the grid spacing to be decreased by half in both directions) together with the corresponding experimental data; results are almost mesh independent, since a little difference exists between coarse and fine grid simulations. Therefore, a non-uniform *384 × 128* grid resolution is good enough to speculate the flow characteristics. Numerical results from the widely-used SST model are also plotted for the comparison purpose. Qualitatively, the "roof-top pressure" is well-captured, the shock location is replicated slightly downstream (with the finer grid) and the "post-shock pressure recovery" on the upper (suction) surface remains poorly predicted compared with experiments. This deficiency could be primarily attributed to the linear eddy-viscosity models that are used without "compressibility corrections".

The C_p (pressure coefficient) distributions on the lower surface (pressure side) remain analogous to the measured profiles for the NSST and SST turbulence models. The C_f (skin-friction) results from both turbulence models align well with measurements and capture a shock-induced separation with a small zone of separation (separated flow), as indicated by Figure. 2(b). Nevertheless, the airfoil C_f distribution of the pressure side does not indicate any flow separation phenomenon. No detailed comments can be made regarding the separation along the pressure side because no experimental data are available at that region. The lift and drag coefficients for the first combination are given in Table 1. The predictive model errors from experiments in C_L and C_D are evaluated as: $\frac{(\phi_{\text{model}} - \phi_{EXPT})}{\phi_{EXPT}} \times 100\%$. The force coefficients predicted by both models are almost identical and maintain a good correspondence with experiments.

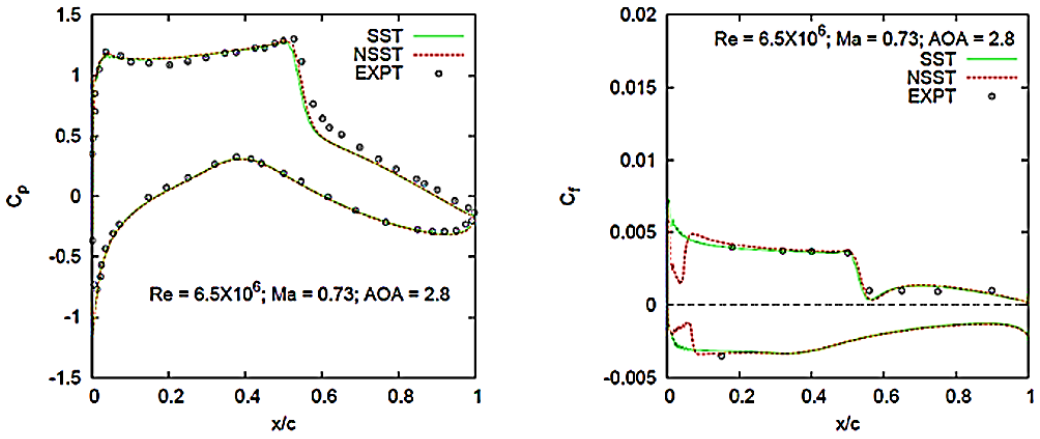

Figure 4: RAE2822 air foil with Ma = 0.73 and AOA= 2.8 deg at$Re_\infty = 6.2 \times 10^6$: (a) $C_p$profiles; (b) $C_f$profiles

Figure 3 illustrates the profiles of pressure and skin-friction coefficient distributions for the second combination of *Re = 6.5 × 10^6, Ma = 0.73 and AOA = 2.51 deg* with measurements. Apparently, the shock location is replicated slightly upstream of the experimental location, the "roof-top pressure" is nicely captured and the "post-shock pressure recovery" is reasonably predicted. The C_p (pressure coefficient) distributions on the lower surface of the airfoil (pressure side) remain identical to experiments. The profiles of C_f (skin-friction coefficient) generated by both representative turbulence models match the measured data well and capture the abrupt change in C_f at the shock location, as indicated by numerical results in Figure. 3(b). However, the shock is too weak to induce separation and therefore, the shock-induced separation is not detected.

Computational results for the third combination of *Re = 6.5 × 10^6, Ma = 0.73 and AOA = 2.8 deg*, accompanied by the measured data are depicted in Figure. 4. Compared to other combinations, both models produce the best predictions of the "roof-top pressure" and pressure recovery along with the shock location behind the shock on the upper (suction) surface. Other aspects are similar to those of the second combination. Interestingly, $C_f$profiles from both NSST and SST models in this combination deeply penetrate to the shock location as demonstrated in Figure. 4(b), showing a tendency to predict the shock-induced separation; this feature can be regarded as "numerical separation".

Table 2 provides comparisons of the calculated lift$C_L$and drag$C_D$coefficients from SST and NSST turbulence models with measurements [2]. As can be seen, the computed values of lift and drag coefficients from both turbulence models make good correspondence with measurements; almost analogous numerical outputs are produced by SST (non-transition) and NSST (transition & non-transition) models. The SST predictions are slightly better than those of the NSST for the second combination; however, lift and drag accuracies of the NSST are superior to the SST with the third combination. Seemingly, the included transition model does not play a major role to precisely compute$C_L$and$C_D$coefficients at a lower *AOA= 2.51* deg in the present set of simulations.

Table 2
RAE2822 airfoil: $\boldsymbol{C_L}$and$\boldsymbol{C_D}$for Ma = 0.73 at$\boldsymbol{Re_\infty = 6.2 \times 10^6}$

AOA	Parameters	EXPT	SST	NSST
2.51 deg	C_L	0.743	0.745	0.750
–	Err (%)	–	0.27	0.94
–	C_D	0.0128	0.0130	0.0131
–	Err (%)	–	1.56	2.34
2.8 deg	C_L	0.803	0.788	0.800
–	Err (%)	–	−1.87	−0.37
–	C_D	0.0168	0.0156	0.0160
–	Err (%)	–	−7.14	−4.76

4. CONCLUSIONS

The RANS modelling still remains as the standard workhorse on the perspective of simulating industrial complex turbulent flows. It requires appropriate selections of the turbulence models/closures, which are vital to accurately accounting for dominant physical flow features like the BL separation and "shock-wave BL interactions". The transonic wall-bounded flow past an RAE2822 airfoil inherits strong "shock-wave BL interactions" with a shock-induced separation. Both the SST and NSST models have been shown to be potential in representing the physics of the flow by comparing model predictions with the measured data. To conclude, the NSST model slightly outperforms the standard SST model with respect to the drag accuracy at a higher AOA. However, employing the NSST transition model plays a minor role to precisely speculate the coefficients of lift and drag in the present simulations, signifying that the NSST model resembles the standard SST model.

Disclosure statement

No potential conflict of interest is reported by the authors.

REFERENCES

Cook, P. H., M. A. McDonald, M. C. P. Firmin, Aerofoil RAE 2822 - Pressure Distributions, and Boundary Layer and Wake Measurements, *in RAE2822 Transonic Airfoil*, J.W. Slater, Editor. 1979: NASA.

Da Ronch, A., et al., Sensitivity and calibration of turbulence model in presence of epistemic uncertainties. *CEAS Aeronautical Journal*, 2019. 11 doi: 10.1007/s13272-019-00389-y.

Hellsten, A. and S. Laine, Extension of k- W Shear-Stress Transport Turbulence Model for Rough-Wall Flows. AIAA Journal, 1998. 36(9): p. 1728-1729 doi: 10.2514/2.7543.

Lien, F.-S., G. Kalitzin, and P. Durbin, RANS modeling for compressible and transitional flows. *Proceedings of the Summer Program*, 1998.

Menter, F., et al., A Correlation-Based Transition Model Using Local Variables—Part I: Model Formulation. ASME J. Turbomach, 2006. 128 doi: 10.1115/1.2184352.

Menter, F. R., Two-equation eddy-viscosity turbulence models for engineering applications. AIAA Journal, 1994. 32(8): p. 1598-1605 doi: 10.2514/3.12149.

Mundell, A. R. G. and D. G. Mabey, Pressure fluctuations caused by transonic shock/boundary-layer interaction. *The Aeronautical Journal*, 2016. 90(897): p. 274-282 doi: 10.1017/S0001924000015864.

Radespiel, R., A cell-vertex multigrid method for the Navier-*Stokes equations*. 1989.

Rumsey, C. L. and V. N. Vatsa, Comparison of the predictive capabilities of several turbulence models. Journal of Aircraft, 1995. 32(3): p. 510-514 doi: 10.2514/3.46749.

Rahman, M. M., Capturing transition and non-transition flows with a new shear stress transport model. *Chinese Journal of Aeronautics*, 2023. 36(3): p. 121-136 doi: https://doi.org/10.1016/j.cja.2022.08.013.

Rahman, M. M., Predicting transition with wall-distance-free SST k-ω model. *Computers & Fluids*, 2023. 250: p. 105704 doi: https://doi.org/10.1016/j.compfluid.2022.105704.

Rahman, M. and Siikonen, T. An Artificial Compressibility Method for Incompressible Flows. *Numerical Heat Transfer Part B - Fundamentals*, 2001. 40 doi: 10.1080/104077901753243188.

Rahman, M. M. and Siikonen, T. A Dual-Dissipation Scheme for Pressure-Velocity Coupling. Numerical Heat Transfer, *Part B: Fundamentals*, 2002. 42(3): p. 231-242 DOI: 10.1080/10407790260233547.

Rahman, M. M. and Siikonen, T. An artificial compressibility method for viscous incompressible and low Mach number flows. *International Journal for Numerical Methods in Engineering*, 2008. 75(11): p. 1320-1340 doi: https://doi.org/10.1002/nme.2302.

Rahman, M. M., Compromising with corrector step of SIMPLE Algorithm. *Mathematics and Computers in Simulation*, 2021. 188: p. 135-163 doi: https://doi.org/10.1016/j.matcom.2021.03.043.

Rahman, M., Rautaheimo, P., and Siikonen, T. Numerical Study of Turbulent Heat Transfer from Confined Impinging Jets Using a Pseudo-compressibility, *Method*. 1997.

Schwamborn D. 1991: Validation of 2D Navier-Stokes codes with respect to turbulence modelling. *Progress report for the third half-year of the EUROVAL project*, part It: RAE 2822 test cases, Institutfur Theoretische Stromungsmechanik, Gottingen, IB 221-91 A 27.

Singh, J. P., An improved Navier-Stokes flow computation of AGARD case-10 flow over RAE2822 airfoil using Baldwin-Lomax model. *Acta Mechanica*, 2001. 151(3): p. 255-263 doi: 10.1007/BF01246922

Slater J. W. RAE2822 Transonic Airfoil: Study #1, *NASA Glenn Research Centre*, Ohio. http://www.grc.nasa.gov/WWW/wind/valid/raetaf/raetaf01/raetaf01.html